High-Performance Multifunctional Graphene Yarns: Toward Wearable All-Carbon Energy Storage Textiles

Seyed Hamed Aboutalebi,[†,∥,*] Rouhollah Jalili,[‡,∥] Dorna Esrafilzadeh,[‡] Maryam Salari,[†,#] Zahra Gholamvand,[§,△] Sima Aminorroaya Yamini,[†] Konstantin Konstantinov,[†,*] Roderick L. Shepherd,[⊥] Jun Chen,[‡] Simon E. Moulton,[‡] Peter Charles Innis,[‡] Andrew I. Minett,[⊥] Joselito M. Razal,[‡] and Gordon G. Wallace[‡]

[†]Institute for Superconducting and Electronic Materials, AIIM Facility, Innovation Campus, University of Wollongong, North Wollongong, NSW 2522, Australia, [‡]Intelligent Polymer Research Institute, ARC Centre of Excellence for Electromaterials Science, AIIM Facility, Innovation Campus, University of Wollongong, North Wollongong, NSW 2522, Australia, [§]School of Biotechnology, Dublin City University, Dublin 9, Ireland, and [⊥]Laboratory for Sustainable Technology, School of Chemical and Biomolecular Engineering, University of Sydney, Sydney NSW 2006, Australia. [∥]S. H. Aboutalebi and R. Jalili contributed equally to this work. [#]Present address: Maryam Salari: Intelligent Polymer Research Institute, ARC Centre of Excellence for Electromaterials Science, AIIM Facility, Innovation Campus, University of Wollongong, North Wollongong, NSW 2522, Australia. [△]Present address: Zahra Gholamvand: Chemical Physics of Low-Dimensional Nanostructures Group, School of Physics, Trinity College, Dublin 2, Ireland.

ABSTRACT The successful commercialization of smart wearable garments is hindered by the lack of fully integrated carbon-based energy storage devices into smart wearables. Since electrodes are the active components that determine the performance of energy storage systems, it is important to rationally design and engineer hierarchical architectures atboth the nano- and macroscale that can enjoy all of the necessary requirements for a perfect electrode. Here we demonstrate a large-scale flexible fabrication of highly porous high-performance multifunctional graphene oxide (GO) and rGO fibers and yarns by taking advantage of the intrinsic soft self-assembly behavior of ultralarge graphene oxide liquid crystalline dispersions. The produced yarns, which are the only practical form of these architectures for real-life device applications, were found to be mechanically robust (Young's modulus in excess of 29 GPa) and exhibited high native electrical conductivity (2508 ± 632 S m^{-1}) and exceptionally high specific surface area (2605 m^2 g^{-1} before reduction and 2210 m^2 g^{-1} after reduction). Furthermore, the highly porous nature of these architectures enabled us to translate the superior electrochemical properties of individual graphene sheets into practical everyday use devices with complex geometrical architectures. The as-prepared final architectures exhibited an open network structure with a continuous ion transport network, resulting in unrivaled charge storage capacity (409 F g^{-1} at 1 A g^{-1}) and rate capability (56 F g^{-1} at 100 A g^{-1}) while maintaining their strong flexible nature.

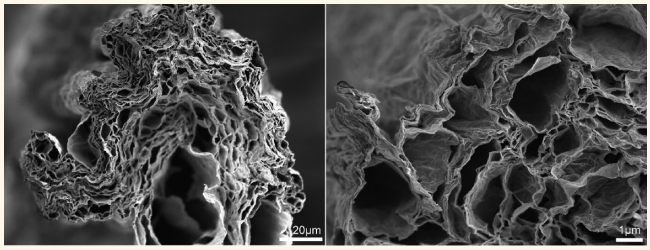

KEYWORDS: supercapacitor · graphene · liquid crystals · self-assembly · multifunctional architectures · fiber · textile

The quest for achieving lightweight, flexible, mechanically strong carbon-based energy storage systems (including but not limited to graphene), as a possible energy source for smart wearable garments and miniaturized electronic gadgets, has necessitated the demand for multifunctional high-performance, cost-effective electrode materials.[1−4] However, most processing methods such as microelectromechanical system technology are not practically scalable and do not yet have the ability to be integrated into commercially feasible processes.[5,6] Nevertheless, the electrochemical capacitance values of such graphene-based devices still fall short of the theoretical value of 550 F g^{-1},[7,8] with values of 265 F g^{-1} per electrode, the best to date.[7]

In this regard, 3D architectures produced from fiber spinning can potentially provide conductive, highly porous 3D frameworks for designing multifunctional microsupercapacitor electrodes.[4,5,9−12] The fibrous architecture is fully scalable for large-scale applications such as integrated flexible and lightweight fabric supercapacitors, which can be further used in smart garments and electronic gadgets.[2,3,5,13−16]

* Address correspondence to konstan@uow.edu.au, sha942@uowmail.edu.au.

Received for review November 21, 2013 and accepted February 11, 2014.

Published online February 11, 2014
10.1021/nn406026z

However, high-performance multifunctional synthetic fibers produced to date, although of interest from a mechanical and electrical point of view, suffer from low electrochemical performance, which is crucial to the realization of multifunctional textiles required for the advancement of smart electronic devices.[11,16−18]

Graphene oxide liquid crystal (LC) dispersions hold great promise in terms of flexibility in processing, high unidirectional properties of the final architectures, and easy integration into complex architectures.[10,19−28] The recent breakthrough in wet-spinning of graphene fibers from graphene oxide LC dispersions is promising as a result of factors including outstanding mechanical and electrical properties, in a cost-effective manufacturing process.[10,25] However, in order to utilize these compelling architectural advances in electronic devices such as wearable electronic textiles and implantable medical devices, highly scalable graphene fibers and yarns with attractive supercapacitor performance need to be developed.

In the present work, we demonstrate that the key to producing such fibers and yarns is to preserve the large sheet size even after the reduction of GO while simultaneously maintaining a high interlayer spacing in between graphene sheets. This in conjunction with maximizing the number of covalently bonded carbon atoms per unit volume or mass and significantly reducing the number of other atoms present at the system and attached to graphene sheets resulted in exceptional electrochemical performance. To achieve this goal, we developed an optimized commercially viable, simple wet-spinning route, followed by an optimal, facile heat-treatment regime to achieve extraordinary capacitance values as high as 409 F g^{-1}/electrode in a practical two-electrode configuration. Both fibers and yarns exhibited outstanding tensile strength and could be easily weaved into conductive textiles, opening up opportunities for the application of graphene in wearable electronic gadgets.

RESULTS AND DISCUSSION

The outstanding mechanical properties of large graphene oxide/graphene sheets suggest the possibility of processing them directly into fibers without the need for a subsequent cross-linking step. The LC spinning technique has this unique advantage in that, without the addition of any binders, it can produce 3D self-assembled and aligned microstructures. To achieve 3D self-assembled, binder-free, aligned microstructures with separated graphene oxide sheets, we present a continuous graphene oxide (GO) fiber spinning method from slightly acidic LC dopants (pH ∼3) in a pure acetone bath. LC GO dispersions were found to be easily spinnable in various wet-spinning methods through spinning of both fibers and yarns (Figure 1). The as-produced fibers could maintain their structural integrity even in the presence of water (Figure1b). The flexibility of the as-prepared fibers was also demonstrated by pulling a tied GO fiber to form an overhand knot. It should be noted that for as-prepared GO fibers spun using acetone the lateral cohesion of the adjacent GO sheets was attributed to the strong van der Waals interactions (from the hydrophobic polyaromatic nanographene domains remaining on the basal planes) and the formation of hydrogen bonds (mediated by the oxygenated functional groups and water molecules).[10,29−31]

The as-prepared GO fibers in the acetone bath exhibited a layered structure, as evidenced by the measured *d*-spacing in X-ray diffraction (XRD) analysis (Figure S1). The high interlayer *d*-spacing in the fiber structure, if preserved, can then serve as a platform to translate the superior properties of graphene sheets into practical everyday use devices with complex geometrical architectures through the prevention of the agglomeration of these sheets at large scale.

In contrast to polymer/ion-containing water-based coagulant baths, the acidic condition of the initial spinning dopant promotes the rate of fiber formation/solidification, resulting in a more porous fiber geometry as detailed in Figure 2. Acetone's advantage in this regard, compared to other coagulants, lies in the ability of acetone to expel water from the fiber at much higher rates, enabling the formation of highly porous architectures (Figure 2b). This is a direct result of its very low viscosity (leading to viscosity difference displacement), high mobility, and high diffusion coefficient compared to water and finally the imbibition rate of acetone compared to other solvents (see Supporting Information for details). Employing slightly acidic GO dispersions (pH ∼3), therefore, leads to more enhanced porosity (Figure 2c). This structure resembles that of a freeze-dried structure due to the very fast dehydration rate of acetone, exhibiting a very high surface area of 2605 m^2 g^{-1} (see Supporting Information for more details).

Furthermore, the enhanced hydrogen bonding between the sheets as a result of the acidic condition and the water molecules confined between the layers plays a crucial role to separate the sheets in the ordered yet porous structures induced by the LC state, as evident from the polarized optical micrograph presented in Figure S2.

However, such a fiber architecture without the reduction of graphene oxide cannot be directly used in electrodes due to the lack of electrical conductivity, which renders it impractical for energy storage applications. However, the reduction of LC GO may result in the restacking of the sheets. Ideally, the restacking should be kept to a minimum to maintain the required interlayer spacing and porosity, as demonstrated by studies on quantum capacitance and ac-line filtering performance, where graphene has been shown to afford much higher storage capacities when individual, separated graphene sheets are predominant.[8,32]

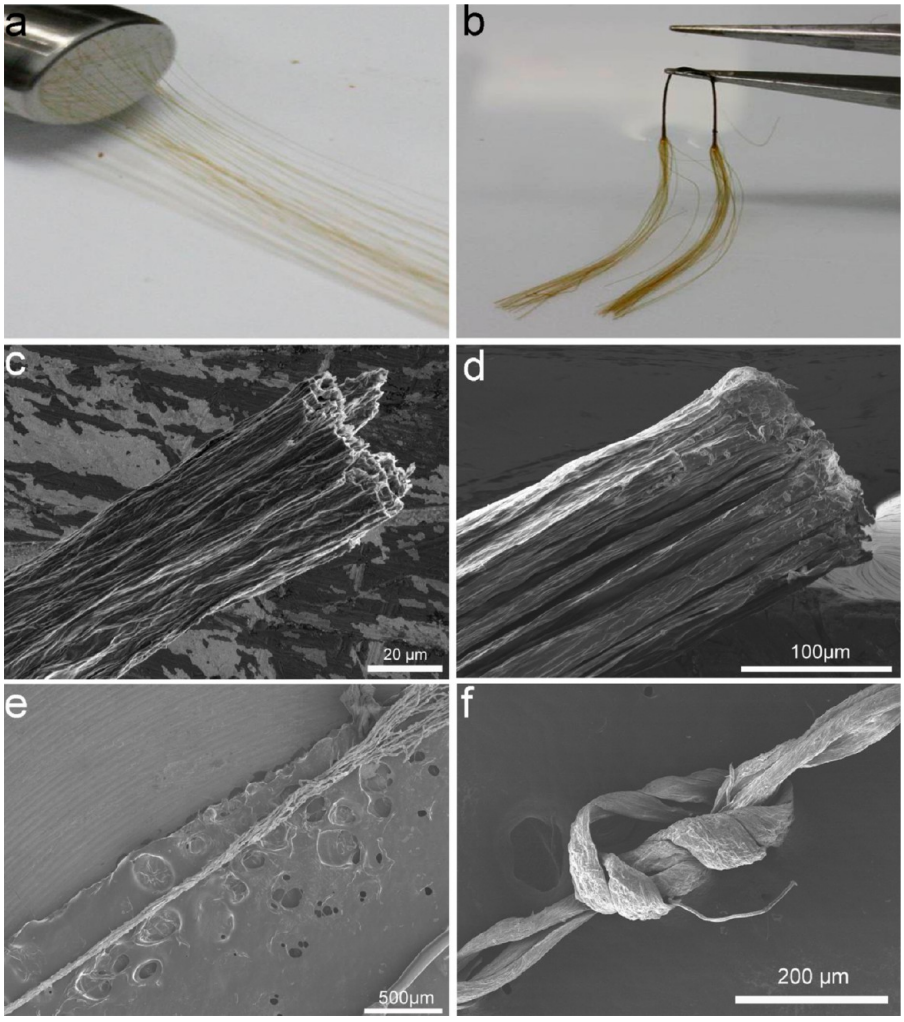

Figure 1. Spinning of GO fibers and yarns. (a) Digital image of the formation of gel-state GO yarns produced using a multihole spinneret. As the LC GO is injected into the coagulation bath, GO filaments are being coagulated instantly by the coagulation solution. (b) Dried GO yarn can be easily separated into individual filaments when they are immersed in water. However, the fibers could still maintain their structural integrity in the presence of water. FESEM micrographs of (c) an irregularly shaped GO fiber, (d) a GO yarn composed of many GO fibers, (e) an unwoven GO fiber yarn, and (f) a loosely knotted GO yarn demonstrating the flexibility of the as-prepared GO fibers in an acetone bath.

Therefore, careful, rational nanoarchitectonic design and spacing of individual graphene layers is crucial for high-performance energy storage devices.[33] To this end, different research groups have implemented various strategies to prevent the restacking of graphene sheets, including introducing carbon nanotubes (CNTs) in between the sheets,[20,29,34] using hydrated chemically converted graphene sheets,[35] and laser scribing of graphene oxide.[7,36] Our strategy here was to heat-treat the as-prepared graphene oxide fibers at an optimal temperature region of 200−220 °C to minimize restacking and maintaining surface area while simultaneously reducing GO sheets, as evidenced by XRD, scanning electron microscopy (SEM), Raman, and X-ray photoelectron spectroscopy (XPS) analysis (Figure 3). Heat-treatment-induced reduction compared to other methods of reduction enables the fine-tuning of the reduction process by simply changing the reduction temperature. Therefore, more control can be exercised on the reduction process while simultaneously keeping a minimum level of multifunctional groups present in the system. These multifunctionalities can then act as pillars, inhibiting the restacking of graphene sheets. The XRD pattern shows a broad distribution of *d*-spacing and pore sizes in the final architecture (from 0.3 to 0.65 nm). This spacing dimension is crucial for the functional design of our reduced graphene oxide (rGO) fibers. This intersheet *d*-spacing was in accordance with self-stacked, solvated graphene (SSG) films, which are known to afford high capacitance values.[35] Pore sizes at this region (less than 1 nm) cannot be directly investigated by BET-N_2 gas adsorption measurements, as these pores are not sufficiently accessible to nitrogen because the filling of the pores takes place at relative pressures of 10^{-7} to 10^{-5} (see Supporting Information for more details).[37,38] Therefore, XRD serves as one of the best techniques to directly probe these pore sizes.

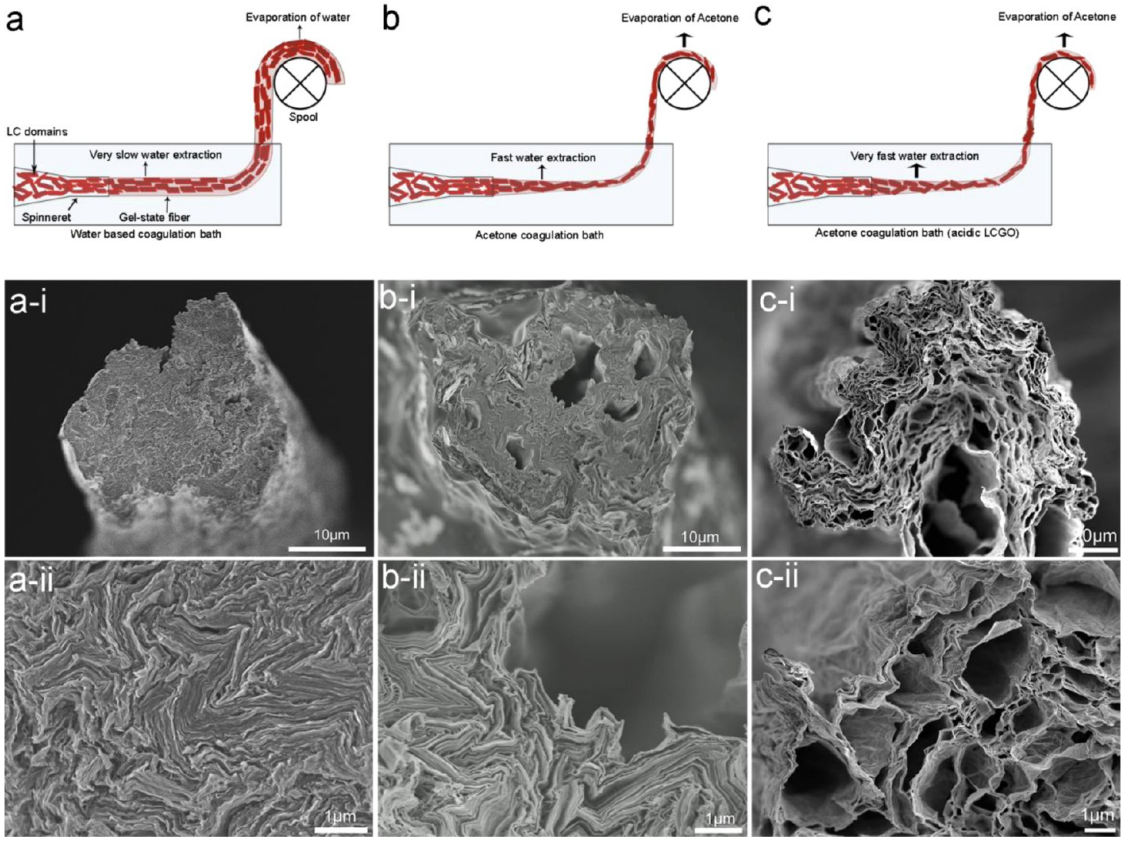

Figure 2. Proposed strategies for the evolution of structure in different coagulation baths from (a) highly dense to (c) highly porous architectures. (a) Employing a water-based coagulation bath results in slow expulsion of water from the as-injected gel-state fiber-like structure. Therefore, to be able to pick up such fibers, the length of the bath should be optimized to enable the formation of a solid-like sheath around the core of the fiber. The fiber can then be taken from the bath and transferred on a spool for the evaporation of the water from the fiber, resulting in a highly dense structure (a-i and a-ii). (b) Using an acetone coagulation bath results in the high rate of water extraction from the surface as a result of the difference in imbibition rate (see Supporting Information for more details), consequently leading to higher rate of solidification and porous fiber structure (b-i and b-ii). (c) The slight acidic condition of LC GO dopants (pH ~3) further changes the difference in imbibition rate, resulting in much higher water extraction rate and consequently more porous geometry (c-i and c-ii).

The higher *d*-spacing value is attributed to the presence of some remaining functionalities on the surface of the reduced graphene oxide fiber after thermal reduction, as described previously and demonstrated in Figure 3C (XPS characterization of as-prepared rGO) and Figures S3 and S4 (XPS and FT-IR characterization of as-prepared GO fibers and rGO). Shown in the spectrum of the annealed rGO fiber after deconvolution of the peaks are the major C in graphite (C 1s A, 284.5 eV) and minor peaks C−OH (C 1s B, 285.6 eV), C═O (C 1s D, 28.2 eV), and C(O)O (C 1s E, 289.4 eV). Quantitatively, from the surveys, upon heat-treatment reduction, the oxygen content fell from 36.6 to 11 wt %. This translates to a carbon to oxygen ratio increase from 0.33 in GO to 0.89 in rGO, indicating the effectiveness of the reduction regime. These observations are in good agreement with literature values for rGOs, where the C content ranges from 60 to 86.4 wt % and the oxygen content ranges from 11.3 to 34.6 wt %.[21,22,39]

Importantly, this reduction regime does not adversely affect the final sheet size of the layers, as evidenced by Figure 3d (electron micrograph of ultralarge rGO sheets in excess of 50 μm) and Figure S5 (high-throughput optical micrograph of rGO sheets). As previously demonstrated by our group and others, fibers from large GO sheets can also give rise to higher electrical and mechanical properties as a result of the reduction of the number of graphene sheet ends in the fiber and reducing graphene junctions like the case with long CNTs.[10,40,41]

Representative stress−strain curves of rGO fibers and spun yarns are compared in Figure 4a. It should be noted that although promising breakthroughs have been made in the case of GO and rGO fibers,[10,42] no reports yet exist on mechanical properties of GO and rGO yarns, which is the only practical form of these structures in real-life applications. The mechanical properties along with the comparison with previous reports on graphene fibers are summarized in Table S1.

It is evident from the results that the employed coagulation bath and reduction of the GO sheets influence the mechanical properties of GO and rGO fibers. Both fibers and yarns fabricated with the method described here demonstrated exceptional tensile

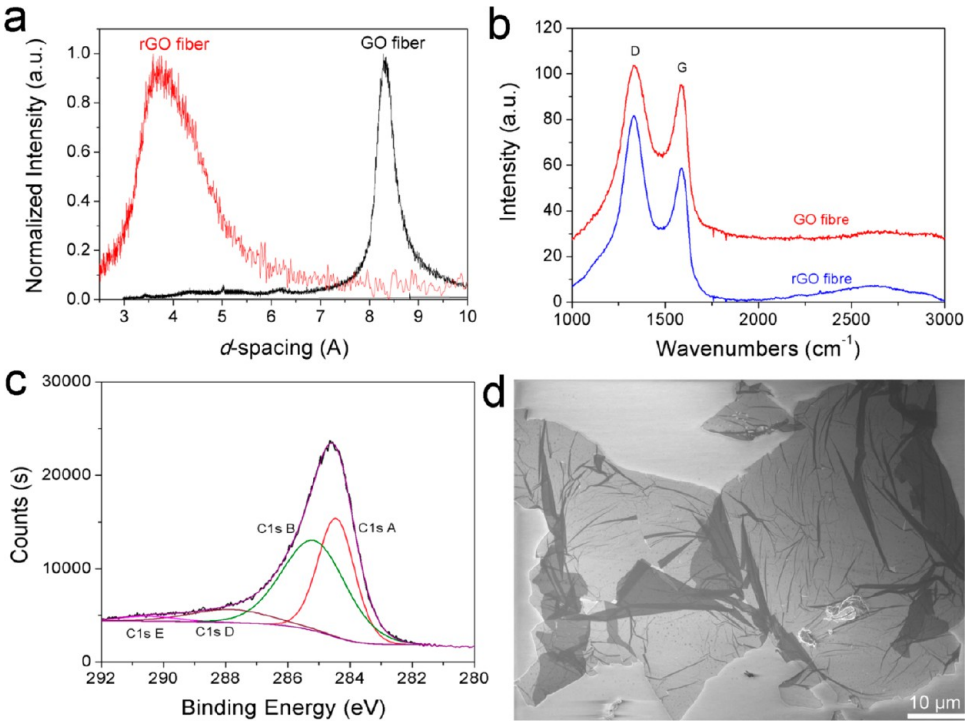

Figure 3. Structural characterization of as-reduced graphene sheets. (a) Comparison of XRD patterns of GO fiber (*d*-spacing ~0.84 nm) and rGO fiber (*d*-spacing in the range of 0.3 to 0.65 nm). (b) Comparative Raman spectra of GO and rGO fiber showing the evolution of the 2D band at around 2600 cm^{-1}, which serves as evidence for the reduction of GO. (c) XPS spectra of the C 1s region of rGO structures after the deconvolution of the peaks. The oxygen content of the rGO was determined to be 11.0% after quantitative measurement from the survey (Figure S4). (d) Representative SEM micrograph of as-heat-treated rGO sheets, verifying the ultralarge nature of our as-prepared rGO.

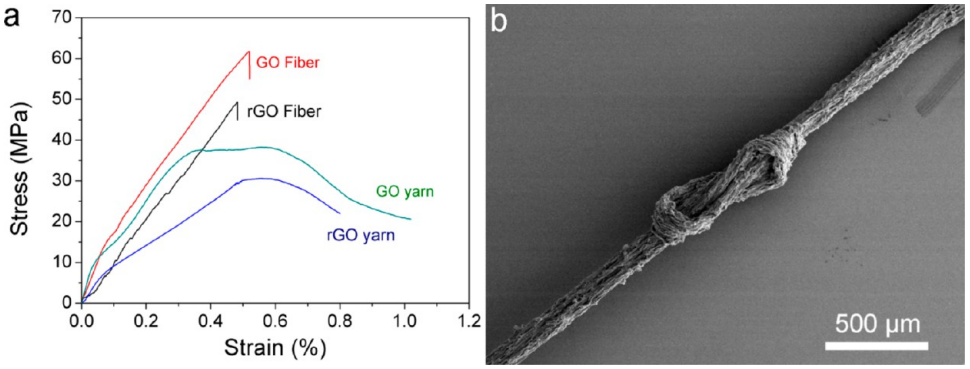

Figure 4. Mechanical performance of fibers and yarns. (a) Representative stress−stain curves of GO and rGO fibers and yarns indicating high tensile strength of all architectures. (b) SEM micrograph of tight-knotted rGO yarns demonstrating mechanical stability of the as-prepared rGO yarns.

modulus, which was indicative of high alignment of GO and reduced graphene sheets in the final architecture. The best GO fiber and yarns' modulus (*ca.* 20.5 and 29.4 GPa, respectively) was even higher than cross-linked GO and rGO-based fibers such as GO fibers coagulated in chitosan (*ca.* 22.6 GPa) and $CaCl_2$ (*ca.* 20.1 GPa) and higher than all of the other previously reported GO and rGO fibers.[10,43,44] This can be explained by the higher degree of hydrogen bonding within the structure, due to the acidic condition in which GO fibers are formed, resulting in stronger interactions between GO sheets. The best rGO fibers and yarns also exhibited higher tensile modulus (*ca.* 10.13 and 10.8 GPa, respectively) compared to rGO fibers reduced by HI acid (*ca.* 5.4 GPa)[42] and partially reduced graphene oxide fibers using NaOH (9 GPa).[10] The results were also comparable with rGO fibers coagulated by NaOH and further reduced at 220 °C (11 GPa) in our previous report.[10] In terms of ultimate stress and elongation at break, these GO and rGO fibers and yarns were inferior to our previous report, which is due to the highly porous architecture of our as-produced fibers and yarns.[10] The annealed rGO fibers also exhibited a native conductivity of *ca.* 2508 ± 632 S m^{-1}, higher than both rGO fibers coagulated by NaOH and laser-scribed rGO, making them suitable for achieving high electrochemical double layer capacitance (EDLC).[7,10]

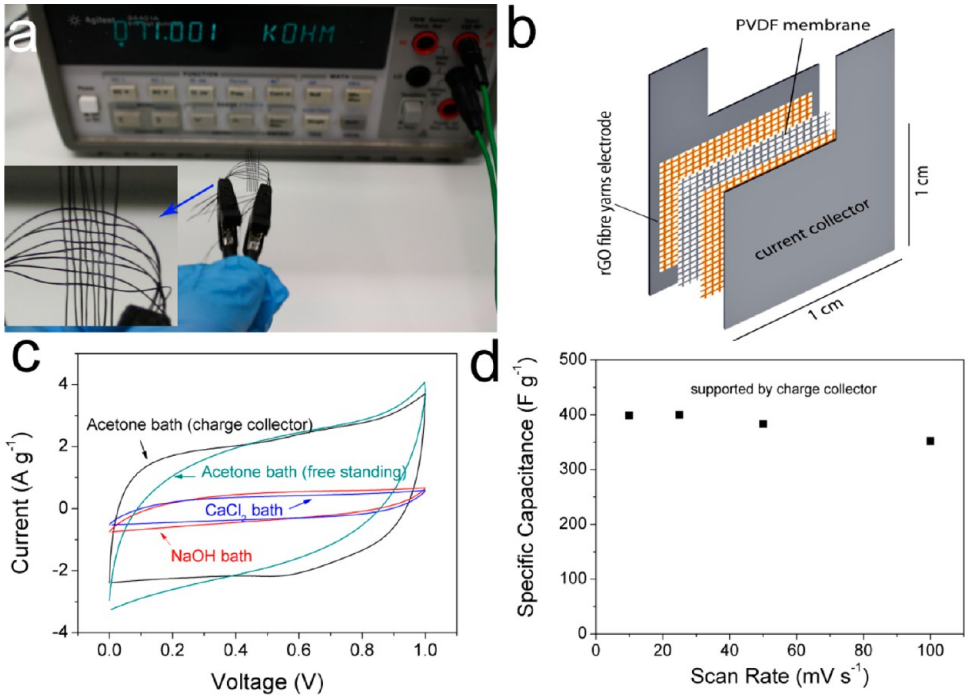

Figure 5. Electrochemical capacitor: design and performance. (a) Hand-weaving of rGO fiber yarns into a flexible and conductive textile. (b) Schematic of the electrochemical capacitor cell assembly fabricated in this study. (c) Cyclic voltammograms of heat-treated graphene fiber yarns produced in an acetone bath (both free-standing and deposited on charge collectors), alkaline bath (NaOH), and ionic cross-linking using a divalent cation bath ($CaCl_2$) in 1 M H_2SO_4 at 10 mV s^{-1} clearly showing the superior performance of the fibers produced in an acetone bath. (d) Calculated specific capacitance of rGO fiber yarns fabricated in an acetone bath at various scan rates.

The mechanical stability and flexibility of these rGO fibers were verified by pulling a tied rGO yarn to form a tight overhand knot (Figure 4b). No breakage occurred when the fiber was curved into a tightened knot. The mechanical stability of these fibers was used to weave different patterns and geometries that are suitable for a range of different applications, including large-area electronics (Figure 5a). This is important for electrochemical capacitor applications and is mainly due to the fact that the need for any additional binders or conductive additives can be eliminated and the as-prepared hand-knitted textile fabricated from graphene fibers can act as both current collector and the active material simultaneously. This design concept can be further used to fabricate porous lightweight textile supercapacitors that can be integrated into smart garments. Devices can be fabricated by simply using a membrane separator in between two textile electrodes (Figure 5b). Other devices can also be made by spinning graphene fiber yarns directly on top of a charge collector or putting these materials onto aluminum or titanium foils that are typically used in commercial devices. As a proof of concept, we prepared a range of different electrodes and devices to evaluate the capacitance performance of these materials, including both free-standing fibers and patterned geometries of graphene fiber yarns on titanium foils fabricated with different methods of wet-spinning: nonsolvent precipitation, dispersion destabilization using acid, base, or salt solutions, and ionic cross-linking using divalent cations with the same reduction regime.

The heat-treated graphene fiber yarns produced in an acetone bath, alkaline bath (NaOH), and ionic cross-linking agents using a divalent cation bath ($CaCl_2$) were all evaluated in terms of electrochemical performance based on their cyclic voltammogram (CV) response at 10 mV s^{-1} (Figures 5c and S6). All systems showed a near-rectangular CV curve representative of good EDLC performance. However, yarns fabricated via wet-spinning of GO dispersions in an acetone bath exhibited a much better electrochemical response (both as a free-standing form or supported by a charge collector, Figure 5c). Use of cross-linking agents results in the addition of impurities to the system and adulteration of carbon bonds, consequently leading to much lower electric double layer capacitance. Wet-spinning of GO dispersions in an acetone bath prevents the adulteration effects of impurities into the system. The adulteration effect of impurity atoms in the case of other coagulant baths is, therefore, the main reason behind the much lower observed electrochemical performance. The compact fiber architectures as shown in Figure 2a, which is a direct result of the slow coagulation/dehydration process, can also adversely affect the electrochemical performance of the fibers, as demonstrated in the cyclic voltammograms presented in Figure 5c.

TABLE 1. Specific Capacitance of rGO Fibers and Yarns Prepared in This Study against Previous Reports on Multifunctional Fibers

production condition	electrolyte	voltage window	specific capacitance (F g^{-1})	ref
rGO yarns coagulated in acetone bath and heat-treated at 220 °C	1 M H_2SO_4	(0−1 V)	409 @ 1 A g^{-1}	current study
			400 @ 25 mV s^{-1}	
twist-spun yarns of nitrogen-doped carbon nanotubes	0.5 M H_2SO_4	(0−1 V)	39 @ 5 mV s^{-1}	17
PEDOT:PSS SWNT composite fiber	$TBABF_4$/acetonitrile	(0−1 V)	59 @ 50 mV s^{-1}	4
ethylene glycol treated PEDOT:PSS fiber	$TBABF_4$/acetonitrile	(0−1 V)	29 @ 20 mV s^{-1} (three-electrode configuration)	9
HA-CNT fiber	0.2 M H_2SO_4	(0−1 V)	44	47
graphene/porous carbon woven film	1 M Na_2SO_4	(0−1 V)	173	18
MnO_2-coated graphene/porous carbon woven film	1 M Na_2SO_4	(0−1 V)	225	18
annealed polymer-free carbon nanotube fibers	ionic liquid−solid	(0−1.5 V)	100	11
carbon microfiber bundles (MWCNTS/Carbon fibers)	water-based gel electrolyte (PVA + H_3PO_4)	(0−1 V)	80 @ 2 mV s^{-1}	48
knitted CF	water-based gel electrolyte (PVA + H_3PO_4)	(0−1 V)	88 @ 10 mV s^{-1}	3
			76 @ 0.4 A g^{-1}	
woven CF	water-based gel electrolyte (PVA + H_3PO_4)	(0−1 V)	63 @ 10 mV s^{-1}	3
			63 @ 0.4 A g^{-1}	
graphene microfibers	H_2SO_4 PVA gel	(0−1 V)	40	16

Therefore, yarns prepared in an acetone bath were chosen for the evaluation of their possible use as supercapacitor electrodes. Calculations for specific capacitance per electrode, energy density, and power density were performed following the methods previously reported.[13,45,46] The as-reduced acetone bath fabricated device showed remarkable electrochemical performance. The free-standing system showed a remarkable capacitance of 394 F g^{-1} (0.99 mF cm^{-1}) at a scan rate of 10 mV s^{-1} (a total capacitance of 40 mF for the device) and continued to provide an outstanding capacitance of 160 at 100 mV s^{-1} (Figures S7 and S8). The capacitive behavior of as-prepared electrodes exhibited low resistivity, as evidenced by the rectangular shape observed in the voltammograms (Figure 5c). However, even this low resistivity can limit the performance of the configurations at faster scan rates, as demonstrated by the high drop in capacitance at higher scan rates. To overcome this problem, devices were fabricated using charge collectors. Employing charge collectors resulted in higher capacitance (399 F g^{-1} at 10 mV s^{-1}). Even at a very high scan rate of 100 mV s^{-1}, an outstanding capacitance of close to 300 F g^{-1} was obtained (Figure 5d and Figures S9 and S10).

With galvanostatic cycling, even at a high current density of 10 A g^{-1}, the *IR* drop at the start of the discharge curve (Figure S11) was negligible, which shows the formation of an efficient EDL with fast ion transport, implying the high rate capability of the as-prepared rGO yarns. Moreover, the negligible *IR* drop at the start of the discharge curve was an indicator of a device with very low equivalent series resistance, as also evidenced by the high native conductivity of *ca.* 2508 ± 632 S m^{-1} of the yarn fibers. A high specific capacitance value of 409 F g^{-1} at a current density of 1 A g^{-1} was obtained, comparable with the specific capacitance values extracted from voltammograms. This capacitance value was much higher than the best microsupercapacitors (∼265 F g^{-1}) and high-performance multifunctional fibers. Table 1 sets the electrochemical capacitance values of our fibers in the context of a range of electrochemical data from high-performance multifunctional fibers in the literature.

The specific capacitance values were calculated over a range of current densities of up to 100 A g^{-1} (Figure 6a and Figures S12 and S13). Graphene fibers continued to provide outstanding EDL capacitance (56 F g^{-1}) at the current density of 100 A g^{-1}, comparable with specific capacitance values of thin film supercapacitors and microdevices at much lower current densities.[1,6] The electrodes were tested for 5000 cycles at a current density of 10 A g^{-1} and showed no visible capacitance loss (Figure 6c).

Substantial effort has been focused toward increasing the energy density of supercapacitors through the use of metal oxides or conducting polymers, which usually comes at the expense of cyclability or power, and they are the governing factors that distinguish supercapacitors from mediocre batteries.[2] Here, through the inducement of an appropriate nanostructure in graphene-based electrodes, we also demonstrate their impressive performance (device power and energy densities of 25 kW kg^{-1} and 14 Wh kg^{-1}, respectively, in a modest potential window of 1 V) when used as flexible textile electrodes (Figure 6d).

Such a performance can be attributed to the increased interlayer spacing, leading to enhanced access

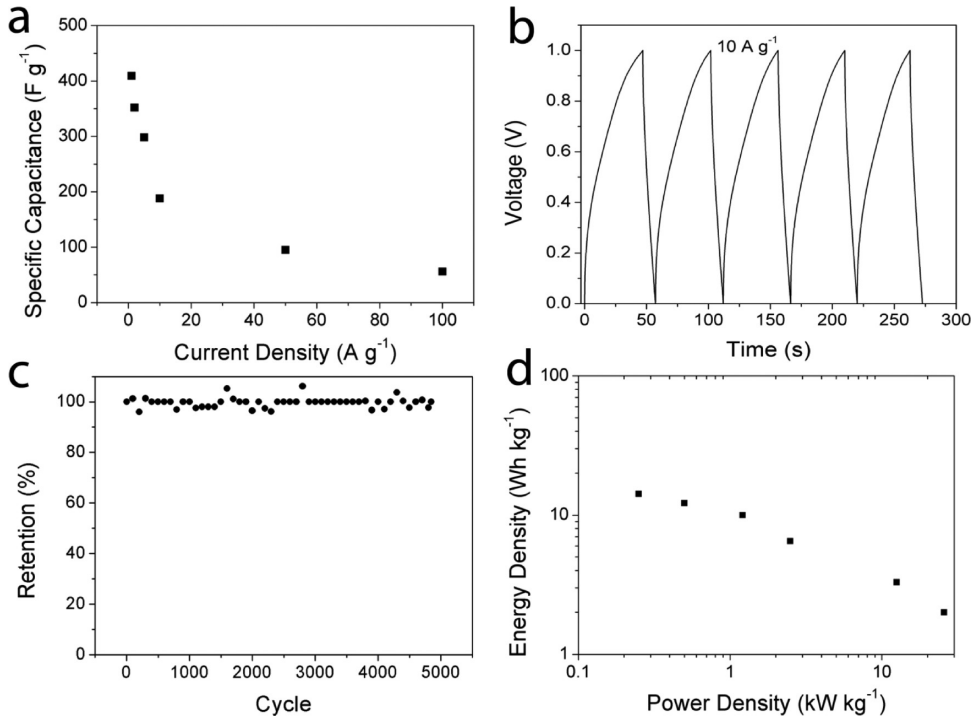

Figure 6. Electrochemical performance of rGO fiber yarns. (a) Supercapacitor performance of rGO fiber yarns in 1 M H_2SO_4 using a two-electrode symmetrical cell showing specific capacitance for each evaluated current density. (b) Galvanostatic charge−discharge curves at constant current density of 10 A g^{-1}. (c) Capacitance retention for 5000 cycles at 10 A g^{-1} current density. (d) Ragone plot for each evaluated current density.

of ions to the interplanar space between the sheets. Furthermore, the sheet size of individual graphene sheets plays a crucial role in achieving high capacitance values, as large sheet size essentially means more uninterrupted surface and less grain boundaries, which are essential for achieving both high conductivity and higher EDL capacitance. The prevention of restacking, as demonstrated in Figure 3a and fiber cross sections (Figure 2c) can result in the easy access of electrolyte ions into the open pores of the structure. As only the surfaces that are in direct contact with the electrolyte contribute to overall capacitance, the open network structure results in the maximum theoretical surface, thus yielding enhanced capacitive performance. The open pores formed within fibers (Figure 2c) that essentially form during the coagulation process and structural freezing and are maintained even after reduction resulted in attaining an extremely high surface area after the reduction of the as-freozen structure (2210 m^2 g^{-1}) and can facilitate the electrolyte accessibility and ionic diffusion in graphene fibers. Such a high surface area is an ideal medium for supercapacitors, as the EDLC is directly proportional to the surface area.[33] This was also verified by the analysis of the cross-section of fibers with FESEM, showing that the intersheet restacking has been effectively prevented (Figure 2c), thus allowing the separate sheets in our multilayered fibers to behave as individual sheets. Furthermore, due to the negative charge buildup on the surface of rGO, it is safe to assume that positive ions, hydronium (H_3O^+) in acidic electrolyte, will be adsorbed on the surface of the working electrode during the charge−discharge process. Acidic solution (H_2SO_4) produces SO_4^{2-} and H_3O^+. In terms of ionic size, the hydrated ionic radius of SO_4^{2-} and H_3O^+ is reported to be 400 and 280 pm, respectively, which is less than the interlayer *d*-spacing of as-prepared rGO yarns (300 to 650 pm). Therefore, this proper spacing in our rGO architecture not only prevents restacking and keeps the surface area high but also provides nanoengineered space for ions to intercalate. Therefore, the rGO fiber architecture provides an excellent platform to accommodate and intercalate both ions, resulting in enhanced capacitance values. According to the Helmholtz formula, small ionic size results in lower charge separation distance; thus higher capacitance in a determined surface area can be realized. Therefore, the combination of both highly accessible surface area and maximizing the number of covalently bonded carbon atoms through spinning in an acetone bath are the contributing factors toward the exceptional performance obtained here.

The key achievement is not only to construct renewable and sustainable energy sources but also, perhaps even more importantly, to store energy efficiently and deliver it on demand, often for mobile applications, such as transportation systems and portable electronic devices. The findings presented here will provide practical solutions for the fabrication of a wide range of large-scale 3D graphene-based architectures (including metallic

or polymer-based composites) with extensive applications in multifunctional wearables, sensors, supercapacitor devices, and electronic gadgets.

CONCLUSION

In summary, flexible, durable, and self-assembled graphene textile electrodes for supercapacitors were fabricated using a novel wet-spinning approach followed by heat-treatment to obtain graphene fibers. The fiber spinning route from ultralarge graphene oxide liquid crystals provided a unique highly porous 3D platform with proper spacing dimensions, which is highly desirable for a range of energy storage applications. The as-prepared material was then used as a building block to fabricate cost-effective high-capacity supercapacitor devices. The electrodes showed unrivaled EDL capacitance performance close to the theoretical capacitance of graphene sheets. The approach is readily scalable and can be used to produce multifunctional flexible yarns. The electrochemical data and capacitances achieved along with high energy density of the devices demonstrate the considerable potential of graphene fiber assemblies in the quest for maximal electrochemical performance. The ease of synthesis and the abundance of the starting material make the use of these architectures an attractive, alternative way of designing next-generation supercapacitors in both conventional fields and new emerging areas.

METHODS

Synthesis of LC GO. The experimental setup and procedure for the synthesis of graphene oxide liquid crystals were based on our previously reported synthesis method.[10,21−23,29] Expandable graphite flakes (3772, Asbury Graphite Mills, US) were thermally treated at 1050 °C for 15 s to produce expanded graphite (EG) and then used as the precursor for graphene oxide synthesis. In a typical GO synthesis, 1 g of EG and 200 mL of sulfuric acid were mixed and stirred in a three-neck flask for 24 h. Five grams of $KMnO_4$ was added to the mixture and stirred at room temperature for 24 h. The mixture was then cooled in an ice bath, and 200 mL of deionized water and 50 mL of H_2O_2 were poured slowly into the mixture, resulting in a color change to light brown followed by stirring for 30 min. The resulting dispersion was washed and centrifuged three times with a HCl solution (9:1 vol water/HCl). Repeated centrifugation−washing steps with deionized water were carried out until a solution of pH ≥6 was achieved. Large GO sheets were redispersed in deionized water by gentle shaking.

Wet-Spinning of GO and rGO Fibers and Yarns. Wet-spinning was carried out using a custom-built wet-spinning apparatus using acetone as a coagulation bath. Wet-spinning of GO fibers using $CaCl_2$ and NaOH coagulation baths was also carried out similar to our previous report.[10] Dried GO fibers were obtained by air-drying under tension at room temperature. Reduction of GO fibers was carried out by overnight annealing at 220 °C under vacuum. In addition to single-filament fiber-spinning, we were also able to demonstrate multifilament spinning to directly prepare GO fiber yarns using a multiorifice spinneret (each orifice diameter is 120 μm).

Characterization of Fibers. SEM analyses were carried out by first depositing GO sheets from their dispersions on precleaned and silanized silicon wafers (300 nm SiO_2 layer). rGO sheets were obtained by annealing graphene oxide sheets deposited on silanized silicon wafers overnight at 220 °C under vacuum. As-deposited rGO sheets were directly examined by scanning electron microscopy (JEOL JSM-7500FA). X-ray diffraction studies were performed using a powder XRD system (Philips1825) with Cu Kα radiation (λ = 0.154 nm) operating at 40 keV and with a cathode current of 20 mA. X-ray photoelectron spectroscopy was carried out on fibers deposited onto a 1 cm^2 silicon wafer and allowed to dry. The XPS spectra were recorded using Al Kα radiation (1486.6 eV). The survey scan was recorded at 0.05 eV s^{-1} at 1 eV resolution and at 0.2 eV s^{-1} at 0.1 eV resolution for the high-resolution regions involving the C and O excitations. The birefringence of the GO fiber was examined by polarized optical microscopy (Leica DM EP) operated in transmission mode.

Supercapacitor Measurements. Supercapacitor performance was investigated using cyclic voltammetry (EDAQ e-corder ADI Instruments) and galvanostatic charge−discharge (CD) (BioLogic Science Instruments VMP3) experiments in a two-electrode setup with rGO fiber yarns deposited on a titanium current collector and separated by a PVDF membrane. The mass of the active material was measured to be 50 μg for the woven yarns. The mass per length of yarns was measured to be 2.5 μg cm^{-1}. It should be noted that the concerns regarding shorter diffusion paths do not apply here, as the thickness of the active material is on the order of 30 μm, which is higher than the cross-section of most graphene-based devices and on the order of the thickness used in commercial cells.[1,7,36,45] Moreover, the advantage of using fibers and yarns lies in the fact that increasing the mass does not adversely affect the diffusion path, as the diffusion path is always limited to the radius of the fiber. Therefore any increase in the mass does not adversely affect the measured capacitance values. All CV and CD data were repeatable, and the data reported were all averaged. To calculate the capacitance from CD curves, the same experimental conditions were also applied on plain charge collectors, and then the resulting capacitance contributions of the metal plates were subtracted before calculating their gravimetric capacitance for the graphene fibers.

Conflict of Interest: The authors declare no competing financial interest.

Acknowledgment. The authors thank the Australian Research Council (ARC) for financial support and the Australian National Fabrication Facility (ANFF) materials node for their provision of research facilities. This work was supported by ARC Discovery Project DP1093952 (K.K. and S.H.A.), ARC Discovery Early Career Research Award DE130100310 (S.A.Y.), ARC Queen Elizabeth II Fellowship (S.E.M.), and ARC Federation Fellowship (G.G.W.). The authors thank Alexandra Satalov for critical reading of the manuscript.

Supporting Information Available: Figures S1 to S5, representative characterization of as-prepared fibers and yarns. Table S1, comparison of mechanical performance data in selected significant previous reports and in this study. Figures S6 to S13, representative electrochemical performance data of the as-produced architectures. Figure S14, total resistance as a function of length showing no deviation from ohm law. Fabrication of the electrodes, explanation on imbibition rate, electrochemical calculations, and surface area measurements. Figure S15, determination of the point of complete cation replacement from the titration curve. Table S2, comparison between surface areas obtained by N_2 adsorption (BET model) and MB absorption techniques. Figure S16, schematic illustration of MB wet adsorption and N_2 dry adsorption mechanism. This material is available free of charge *via* the Internet at http://pubs.acs.org.

REFERENCES AND NOTES

1. Pech, D.; Brunet, M.; Durou, H.; Huang, P.; Mochalin, V.; Gogotsi, Y.; Taberna, P.-L.; Simon, P. Ultrahigh-Power

Micrometre-Sized Supercapacitors Based on Onion-Like Carbon. *Nat. Nanotechnol.* **2010**, *5*, 651–654.
2. Jost, K.; Perez, C. R.; McDonough, J. K.; Presser, V.; Heon, M.; Dion, G.; Gogotsi, Y. Carbon Coated Textiles for Flexible Energy Storage. *Energy Environ. Sci.* **2011**, *4*, 5060–5067.
3. Jost, K. A.; Stenger, D.; Perez, C. R.; McDonough, J.; Lian, K.; Gogotsi, Y.; Dion, G. Knitted and Screen Printed Carbon-Fiber Supercapacitors for Applications in Wearable Electronics. *Energy Environ. Sci.* **2013**, *6*, 2698–2705.
4. Jalili, R.; Razal, J. M.; Wallace, G. G. Exploiting High Quality Pedot:Pss-Swnt Composite Formulations for Wet-Spinning Multifunctional Fibers. *J. Mater. Chem.* **2012**, *22*, 25174–25182.
5. Lee, J. A.; Shin, M. K.; Kim, S. H.; Cho, H. U.; Spinks, G. M.; Wallace, G. G.; Lima, M. D.; Lepró, X.; Kozlov, M. E.; Baughman, R. H. Ultrafast Charge and Discharge Biscrolled Yarn Supercapacitors for Textiles and Microdevices. *Nat. Commun.* **2013**, *4*, 1970.
6. Gao, W.; Singh, N.; Song, L.; Liu, Z.; Reddy, A. L. M.; Ci, L.; Vajtai, R.; Zhang, Q.; Wei, B.; Ajayan, P. M. Direct Laser Writing of Micro-Supercapacitors on Hydrated Graphite Oxide Films. *Nat. Nanotechnol.* **2011**, *6*, 496–500.
7. El-Kady, M. F.; Strong, V.; Dubin, S.; Kaner, R. B. Laser Scribing of High-Performance and Flexible Graphene-Based Electrochemical Capacitors. *Science* **2012**, *335*, 1326–1330.
8. Xia, J.; Chen, F.; Li, J.; Tao, N. Measurement of the Quantum Capacitance of Graphene. *Nat. Nanotechnol.* **2009**, *4*, 505–509.
9. Jalili, R.; Razal, J. M.; Innis, P. C.; Wallace, G. G. One-Step Wet-Spinning Process of Poly(3,4-Ethylenedioxythiophene): Poly(Styrenesulfonate) Fibers and the Origin of Higher Electrical Conductivity. *Adv. Funct. Mater.* **2011**, *21*, 3363–3370.
10. Jalili, R.; Aboutalebi, S. H.; Esrafilzadeh, D.; Shepherd, R. L.; Chen, J.; Aminorroaya-Yamini, S.; Konstantinov, K.; Minett, A. I.; Razal, J. M.; Wallace, G. G. Scalable One-Step Wet-Spinning of Graphene Fibers and Yarns from Liquid Crystalline Dispersions of Graphene Oxide: Towards Multifunctional Textiles. *Adv. Funct. Mater.* **2013**, *10*, 5345–5354.
11. Kozlov, M. E.; Capps, R. C.; Sampson, W. M.; Ebron, V. H.; Ferraris, J. P.; Baughman, R. H. Spinning Solid and Hollow Polymer-Free Carbon Nanotube Fibers. *Adv. Mater.* **2005**, *17*, 614–617.
12. Jalili, R.; Razal, J. M.; Wallace, G. G. Wet-Spinning of Pedot: Pss/Functionalized-Swnts Composite: A Facile Route toward Production of Strong and Highly Conducting Multifunctional Fibers. *Sci. Rep.* **2013**, *3*, 3438.
13. Hu, L.; Pasta, M.; Mantia, F. L.; Cui, L.; Jeong, S.; Deshazer, H. D.; Choi, J. W.; Han, S. M.; Cui, Y. Stretchable, Porous, and Conductive Energy Textiles. *Nano Lett.* **2010**, *10*, 708–714.
14. Yu, G.; Hu, L.; Vosgueritchian, M.; Wang, H.; Xie, X.; McDonough, J. R.; Cui, X.; Cui, Y.; Bao, Z. Solution-Processed Graphene/MnO_2 Nanostructured Textiles for High-Performance Electrochemical Capacitors. *Nano Lett.* **2011**, *11*, 2905–2911.
15. Bao, L.; Li, X. Towards Textile Energy Storage from Cotton T-Shirts. *Adv. Mater.* **2012**, *24*, 3246–3252.
16. Meng, Y.; Zhao, Y.; Hu, C.; Cheng, H.; Hu, Y.; Zhang, Z.; Shi, G.; Qu, L. All-Graphene Core-Sheath Microfibers for All-Solid-State, Stretchable Fibriform Supercapacitors and Wearable Electronic Textiles. *Adv. Mater.* **2013**, *25*, 2326–2331.
17. Lepró, X.; Ovalle-Robles, R.; Lima, M. D.; Elías, A. L.; Terrones, M.; Baughman, R. H. Catalytic Twist-Spun Yarns of Nitrogen-Doped Carbon Nanotubes. *Adv. Funct. Mater.* **2012**, *22*, 1098–1098.
18. Li, X.; Zang, X.; Li, Z.; Li, X.; Li, P.; Sun, P.; Lee, X.; Zhang, R.; Huang, Z.; Wang, K.; *et al*. Large-Area Flexible Core–Shell Graphene/Porous Carbon Woven Fabric Films for Fiber Supercapacitor Electrodes. *Adv. Funct. Mater.* **2013**, *23*, 4862–4869.
19. Mohsen, M. G.; Hamed, A. S.; Nariman, Y.; Bin, Z. Q.; Farhad, S.; Jie, C.; Yayun, L.; Allison, X.; Jang-Kyo, K. In *Self-Aligned Graphene Sheets-Polyurethane Nanocomposites*; MRS Proceedings, **2011**; Cambridge University Press, 2011; pp mrss11–1344–y02–06.
20. Yousefi, N.; Gudarzi, M. M.; Zheng, Q.; Aboutalebi, S. H.; Sharif, F.; Kim, J.-K. Self-Alignment and High Electrical Conductivity of Ultralarge Graphene Oxide-Polyurethane Nanocomposites. *J. Mater. Chem.* **2012**, *22*, 12709–12717.
21. Aboutalebi, S. H.; Gudarzi, M. M.; Zheng, Q. B.; Kim, J.-K. Spontaneous Formation of Liquid Crystals in Ultralarge Graphene Oxide Dispersions. *Adv. Funct. Mater.* **2011**, *21*, 2978–2988.
22. Aboutalebi, S. H.; Aminorroaya-Yamini, S.; Nevirkovets, I.; Konstantinov, K.; Liu, H. K. Enhanced Hydrogen Storage in Graphene Oxide-Mwcnts Composite at Room Temperature. *Adv. Energy Mater.* **2012**, *2*, 1439–1446.
23. Jalili, R.; Aboutalebi, S. H.; Esrafilzadeh, D.; Konstantinov, K.; Moulton, S. E.; Razal, J. M.; Wallace, G. G. Organic Solvent-Based Graphene Oxide Liquid Crystals: A Facile Route toward the Next Generation of Self-Assembled Layer-by-Layer Multifunctional 3d Architectures. *ACS Nano* **2013**, *7*, 3981–3990.
24. Kim, J. E.; Han, T. H.; Lee, S. H.; Kim, J. Y.; Ahn, C. W.; Yun, J. M.; Kim, S. O. Graphene Oxide Liquid Crystals. *Angew. Chem., Int. Ed.* **2011**, *50*, 3043–3047.
25. Jalili, R.; Aboutalebi, S. H.; Esrafilzadeh, D.; Konstantinov, K.; Razal, J. M.; Moulton, S. E.; Wallace, G. G. Formation and Processability of Liquid Crystalline Dispersions of Graphene Oxide. *Mater. Horiz.* **2014**, *1*, 87–91.
26. Naficy, S.; Jalili, R.; Aboutalebi, S. H.; Gorkin, R.; Konstantinov, K.; Innis, P. C.; Spinks, G. M.; Poulin, P.; Wallace, G. Graphene Oxide Dispersions: Tuning Rheology to Enable Fabrication. *Mater. Horiz.* **2014**, 10.1039/c3mh00144j.
27. Chidembo, A. T.; Aboutalebi, S. H.; Konstantinov, K.; Jafta, C. J.; Liu, H. K.; Ozoemena, K. I. *In Situ* Engineering of Urchin-Like Reduced Graphene Oxide-Mn_2O_3-Mn_3O_4 Nanostructures for Supercapacitors. *RSC Adv.* **2014**, *4*, 886–892.
28. Chidembo, A. T.; Aboutalebi, S. H.; Konstantinov, K.; Wexler, D.; Liu, H. K.; Dou, S. X. Liquid Crystalline Dispersions of Graphene-Oxide-Based Hybrids: A Practical Approach towards the Next Generation of 3d Isotropic Architectures for Energy Storage Applications. *Part. Part. Syst. Charact.* **2014**, 10.1002/ppsc.201300254.
29. Aboutalebi, S. H.; Chidembo, A. T.; Salari, M.; Konstantinov, K.; Wexler, D.; Liu, H. K.; Dou, S. X. Comparison of Go, Go/Mwcnts Composite and Mwcnts as Potential Electrode Materials for Supercapacitors. *Energy Environ. Sci.* **2011**, *4*, 1855–1865.
30. Cote, L. J.; Kim, J.; Zhang, Z.; Sun, C.; Huang, J. Tunable Assembly of Graphene Oxide Surfactant Sheets: Wrinkles, Overlaps and Impacts on Thin Film Properties. *Soft Matter* **2010**, *6*, 6096–6101.
31. Guo, F.; Kim, F.; Han, T. H.; Shenoy, V. B.; Huang, J.; Hurt, R. H. Hydration-Responsive Folding and Unfolding in Graphene Oxide Liquid Crystal Phases. *ACS Nano* **2011**, *5*, 8019–8025.
32. Miller, J. R.; Outlaw, R. A.; Holloway, B. C. Graphene Double-Layer Capacitor with Ac Line-Filtering Performance. *Science* **2010**, *329*, 1637–1639.
33. Pumera, M. Graphene-Based Nanomaterials for Energy Storage. *Energy Environ. Sci.* **2011**, *4*, 668–674.
34. Yu, D.; Dai, L. Self-Assembled Graphene/Carbon Nanotube Hybrid Films for Supercapacitors. *J. Phys. Chem. Lett.* **2009**, *1*, 467–470.
35. Yang, X.; Zhu, J.; Qiu, L.; Li, D. Bioinspired Effective Prevention of Restacking in Multilayered Graphene Films: Towards the Next Generation of High-Performance Supercapacitors. *Adv. Mater.* **2011**, *23*, 2833–2838.
36. El-Kady, M. F.; Kaner, R. B. Scalable Fabrication of High-Power Graphene Micro-Supercapacitors for Flexible and on-Chip Energy Storage. *Nat. Commun.* **2013**, *4*, 1475.
37. de Jonge, H.; Mittelmeijer-Hazeleger, M. C. Response to Comment on "Adsorption of Co_2 and N_2 on Soil Organic Matter: Nature of Porosity, Surface Area, and Diffusion Mechanisms. *Environ. Sci. Technol.* **1996**, *30*, 3636–3637.
38. de Jonge, H.; Mittelmeijer-Hazeleger, M. C. Adsorption of Co_2 and N_2 on Soil Organic Matter: Nature of Porosity,

Surface Area, and Diffusion Mechanisms. *Environ. Sci. Technol.* **1996**, *30*, 408–413.
39. Gao, W.; Alemany, L. B.; Ci, L.; Ajayan, P. M. New Insights into the Structure and Reduction of Graphite Oxide. *Nat. Chem.* **2009**, *1*, 403–408.
40. Behabtu, N.; Young, C. C.; Tsentalovich, D. E.; Kleinerman, O.; Wang, X.; Ma, A. W. K.; Bengio, E. A.; ter Waarbeek, R. F.; de Jong, J. J.; Hoogerwerf, R. E.; *et al.* Strong, Light, Multifunctional Fibers of Carbon Nanotubes with Ultrahigh Conductivity. *Science* **2013**, *339*, 182–186.
41. Koziol, K.; Vilatela, J.; Moisala, A.; Motta, M.; Cunniff, P.; Sennett, M.; Windle, A. High-Performance Carbon Nanotube Fiber. *Science* **2007**, *318*, 1892–1895.
42. Xu, Z.; Sun, H.; Zhao, X.; Gao, C. Ultrastrong Fibers Assembled from Giant Graphene Oxide Sheets. *Adv. Mater.* **2013**, *25*, 188–193.
43. Xu, Z.; Gao, C. Graphene Chiral Liquid Crystals and Macroscopic Assembled Fibres. *Nat. Commun.* **2011**, *2*, 571.
44. Dong, Z.; Jiang, C.; Cheng, H.; Zhao, Y.; Shi, G.; Jiang, L.; Qu, L. Facile Fabrication of Light, Flexible and Multifunctional Graphene Fibers. *Adv. Mater.* **2012**, *24*, 1856–1861.
45. Zhu, Y.; Murali, S.; Stoller, M. D.; Ganesh, K. J.; Cai, W.; Ferreira, P. J.; Pirkle, A.; Wallace, R. M.; Cychosz, K. A.; Thommes, M.; *et al.* Carbon-Based Supercapacitors Produced by Activation of Graphene. *Science* **2011**, *332*, 1537–1541.
46. Zhang, L. L.; Zhao, X. S. Carbon-Based Materials as Supercapacitor Electrodes. *Chem. Soc. Rev.* **2009**, *38*, 2520–2531.
47. Razal, J. M.; Gilmore, K. J.; Wallace, G. G. Carbon Nanotube Biofiber Formation in a Polymer-Free Coagulation Bath. *Adv. Funct. Mater.* **2008**, *18*, 61–66.
48. Le, V. T.; Kim, H.; Ghosh, A.; Kim, J.; Chang, J.; Vu, Q. A.; Pham, D. T.; Lee, J.-H.; Kim, S.-W.; Lee, Y. H. Coaxial Fiber Supercapacitor Using All-Carbon Material Electrodes. *ACS Nano* **2013**, *7*, 5940–5947.